ANSTO/E662

ANSTO/E662

AUSTRALIAN NUCLEAR SCIENCE AND TECHNOLOGY ORGANISATION

LUCAS HEIGHTS RESEARCH LABORATORIES

OPTIMISATION OF AN EPITHERMAL BEAM IN HIFAR FOR BORON NEUTRON-CAPTURE THERAPY

by

B.V. HARRINGTON

AUGUST 1987

ISBN 0 642 59866 5

AUSTRALIAN NUCLEAR SCIENCE
AND TECHNOLOGY ORGANISATION

LUCAS HEIGHTS RESEARCH LABORATORIES

OPTIMISATION OF AN EPITHERMAL BEAM IN HIFAR FOR BORON NEUTRON-CAPTURE THERAPY

by

B.V. HARRINGTON

ABSTRACT

A calculational study was undertaken to investigate the feasibility of developing an epithermal beam in the 10H horizontal facility of the HIFAR research reactor suitable for boron neutron-capture therapy of deep-seated metastatic melanoma. The filters considered were Al, Al/S and AlF_3. Dose intensities and therapeutic gains in a phantom were calculated to determine optimum neutron and gamma filter lengths.

National Library of Australia card number and ISBN 0 642 59866 5

The following descriptors have been selected from the INIS Thesaurus to describe the subject content of this report for information retrieval purposes. For further details please refer to IAEA-INIS-12 (INIS: Manual for Indexing) and IAEA-INIS-13 (INIS: Thesaurus) published in Vienna by the International Atomic Energy Agency.

ALUMINIUM; ALUMINIUM FLUORIDES; BORON; BORON 10; EPITHERMAL NEUTRONS; FILTERS; DEPTH DOSE DISTRIBUTIONS; GAMMA RADIATION; GAMMA SPECTRA; LITHIUM 7; MELANOMAS; METASTASES; NEUTRON CAPTURE THERAPY; NEUTRON SPECTRA; PHANTOMS; SULFUR; THERMAL NEUTRONS; THERMAL SHIELDS

EDITORIAL NOTE

From 27 April 1987, the Australian Atomic Energy Commission (AAEC) is replaced by Australian Nuclear Science and Technology Organisation (ANSTO). Serial numbers for reports with an issue date after April 1987 have the prefix ANSTO with no change of the symbol (E, M, S or C) or numbering sequence.

CONTENTS

1. INTRODUCTION

The boron neutron-capture therapy (BNCT) of melanoma depends on the selective loading of the tumour with an enriched ^{10}B compound and subsequent irradiation with thermal neutrons. The high thermal cross section for the $^{10}B(n,\alpha)^{7}Li$ reaction means a high production rate of α and ^{7}Li particles. These charged particles have ranges in tissue of <10 μm, hence most of the energy generated in the tumour cell is absorbed within that cell.

For the BNCT of deep-seated metastatic melanoma, an epithermal neutron beam is considered to be superior to a thermal beam because of its deeper penetration and skin-sparing properties. Such a beam would be thermalised within the tissue itself. The kinetic energy released in tissue (kerma) by neutrons has a broad minimum in the eV to low keV range (**figure 1**). Zamenhof *et al.* [1975] and McGregor and Allen [1983] calculated dose-depth distributions in a phantom and showed that epithermal neutron beams in the eV to low keV range have close to optimal characteristics for boron neutron-capture therapy.

The production of monoenergetic beams using a resonance window filter such as Sc (2 keV) involves intensity losses owing to the narrow band of neutrons selected and the inevitable attenuation even of the neutrons in that band. It is unlikely that a suitable monoenergetic beam of sufficient intensity for BNCT can be designed for the reactor HIFAR. The intensities of intermediate energy beams reported by Mill and Harvey [1978] seem to support this. A possible exception is the 24.5 keV beam using an iron filter [Constantine *et al.* 1986]. However, for BNCT a beam ranging in energy through the eV to low keV range could be suitable provided that the fast neutron and gamma contamination levels were not too high. Oka *et al.* [1981] in their design study of an epithermal beam chose a mixture of heavy water and aluminium as suitable for attenuating the fast neutron flux relative to the epithermal flux. Noonan and Russell [1983] used aluminium and sulphur to build their epithermal beam in the Georgia Institute of Technology research reactor. Aluminium and sulphur have the unusual property that their total cross sections are higher above about 30 keV than at lower energies. The advantage is that because of the broader spectrum of the neutron beam produced, it may be possible to achieve a beam of sufficient intensity for boron neutron-capture therapy. The approach in this study has been to consider Al, Al/S and AlF_3 filters for the production of an epithermal beam in the HIFAR horizontal facility 10H. Fluorine was considered because it has an inelastic scattering cross section with a relatively low threshold (~ 100 keV). The horizontal facility 10H was chosen because of its large diameter (28 cm). The calculations addressed two problems:

- the neutron and gamma spectra of the tailored beams, and
- dose-depth distributions in a tissue-equivalent phantom to enable evaluation of the beam.

The dose-depth calculations were used to determine the filter type and length which optimise the dose to the tumour relative to the maximum dose to healthy tissue. Similarly the optimum thickness of the lithium fluoride (^{6}LiF) tile thermal neutron shield and that of either a lead or bismuth gamma shield were determined. The advantage of a tangential beam with its lower gamma and fast neutron components, compared with the radial 10H beam, was also investigated. Some preliminary calculations were reported [Allen *et al.* 1986].

2. HIFAR AND THE 10H HORIZONTAL FACILITY

The materials testing reactor HIFAR is a 10 MW D_2O moderated and cooled reactor of the DIDO class. The core and heavy water are contained in an aluminium tank which is 2 m in diameter and surrounded by a graphite cylinder. The graphite cylinder is supported by a steel tank and surrounded by a biological shield. The 10H horizontal experimental facility is a radial facility at the core mid-plane. A re-entrant aluminium thimble is welded to the reactor aluminium tank and protrudes into the heavy water. The thimble contains a stainless steel liner which in turn contains a cylindrical collimator. An improvement in beam intensity may be achievable by the use of a conical collimator but as extra gamma and thermal neutron shielding would be required it is likely to be less than a factor of 10. The reactor HIFAR and the 10H horizontal facility are shown in **figures 2** and **3**, respectively. In this study the AlF_3, Al and Al/S filters were assumed to be in the core end of 10H as shown in **figure 3**. Calculations with the filter placed at the outer end of the thimble have not been undertaken because of complexity but would determine whether any improvements can be achieved in therapeutic gain or dose intensity. The use of a conceptual filter, not confined to 10H but with a much larger diameter, possibly conical in shape, could be superior but has not been considered in this study.

3. NEUTRON AND GAMMA SPECTRA CALCULATIONS OF THE BEAM

Transport calculations were undertaken to determine the neutron and gamma spectra at the reactor face, resulting from various filters in the 10H facility, as a function of filter length. The ORNL two-dimensional discrete ordinates transport code DOT [Rhoades and Mynatt 1973] was used, and Al, Al/S, AlF_3 filters were considered. As cross-section data for sulphur are not available in the ENDF/B library [Garber 1975], the initial calculations were done using an AUS cross-section library derived from the EPR coupled neutron and gamma cross-section data [Ford *et al.* 1976]. From these calculations it was deduced that Al, Al/S and AlF_3 filters were similar in performance but that, for a given tumour dose, AlF_3 generated a slightly lower gamma dose. Hence AlF_3 was chosen for further study and a 200 group cross-section library derived from ENDF/B-IV data was used.

Because of the fine structure in the Al cross-section data in the resonance region and the changing spectrum along the length of the filter, the calculations were done in 80 energy groups (68 neutron and 12 gamma groups). The group structure used is given in **tables 1** and **2**. An unorthodox cylindrical HIFAR model was used with the axis of 10H as the axis of the cylinder (**figure 4**). Modules of the AUS neutronics system [Robinson 1975] were used to generate 80 group cross sections. The HIFAR fuel cell model BVHIFCEL [Harrington 1983] was used (but with fission products omitted) to produce core cross sections. The 80-group graphite and D_2O cross-section data were produced using the AUS module MIRANDA [Robinson 1977] to condense over the spectrum resulting from a ^{235}U fission source in each material. The AlF_3 cross-section data were obtained by condensing over the calculated flux spectrum in D_2O.

The size of the 80-group transport calculation, including the reactor core, beam tube and graphite region, led to its treatment as the following three overlapping calculations:

(a) A two-dimensional diffusion calculation of the HIFAR model (**figure 4**), normalised to 10 MW thermal with the AUS code POW [Pollard 1974], was used to generate a neutron source representation of the core to be used as input in the transport calculation (b).

(b) A two-dimensional source calculation, using the transport code DOT, was used to generate angular boundary fluxes for two interior boundaries (dotted lines in **figure 4**). A coarse spatial mesh structure, third order Legendre polynomial P_3 scattering treatment and S_{16} angular quadrature were used. The ENDF/B cross-section data for ^{235}U include only the prompt γ-rays released in fission and not the equilibrium fission product gammas which account for approximately 50 per cent of core gammas in HIFAR. In this calculation equilibrium fission product gammas were included as part of the input source, using the fission gamma yield data provided for the PWR shielding benchmark [Hehn 1983].

(c) The angular boundary fluxes from (b) were used as DOT input in a two-dimensional, P_3, S_{16}, fine mesh source calculation of the area enclosed by the dotted lines of **figure 4**. The calculations assumed that the filter material in the 10H facility extended to the edge of the graphite. The angular fluxes were read off at a point on the filter axis, a distance d from the core end of the 10H facility, to obtain the flux spectrum emerging from a filter of a given length d.

It was assumed that a collimator tube with a square 5.08 x 5.08 cm beam hole of length 235 cm extends from the reactor aluminium tank to the reactor face (**figure 3**). Using an equivalent collimator hole radius, r, of 2.87 cm, the ratio of collimator length, z, to radius is 82. For such a large ratio it is reasonable to assume, particularly for epithermal and thermal neutrons, that the flux reaching the outer end of the collimator is the direct (non-wall-reflected) flux which has entered the duct through its inlet mouth. Hence a line-of-sight attenuation factor of $r^2/(4z^2)$ was used to determine the neutron and gamma flux at the outer end of the collimator. Experimental data for ducts [Jaeger *et al.* 1986] suggest that this could produce an uncertainty of up to 25 per cent for the fast neutron flux; furthermore, as the line-of-sight attenuation factor does not take into account gamma build-up factors, the gamma dose will be underestimated.

4. PHANTOM DOSE-DEPTH CALCULATIONS

Dose as a function of depth in a phantom was calculated for the beams derived in the previous section assuming 10 MW reactor power. A ^6LiF thermal neutron shield and a gamma shield (Pb or Bi), were included between the beam and the phantom (**figure 5**). The tissue equivalent phantom head model of Zamenhof *et al.* [1975], which does not individually model the tumour and healthy tissue, was used; the composition is given in **table 3**. Neutron and gamma fluxes resulting from beams incident on the 30 cm deep

tissue equivalent rectangular slab, having a transverse dimension of 13.9 cm to account for transverse leakage, were calculated using the ORNL one-dimensional transport code ANISN [Engle 1967].

Boron-10 was not specifically included in the model but neutron kerma factors for the $^{10}B(n,\alpha)^{7}Li$ reaction were used to calculate tumour and tissue doses for various ^{10}B loadings as a function of depth in the phantom. To check the validity of this approach, the calculation was repeated with 1 μg ^{10}B g^{-1} of tissue included in the phantom. The thermal flux depression in the phantom caused by the ^{10}B was found to be approximately 0.3 per cent near the surface of the skin where the maximum dose to tissue occurs. Thermal neutron flux depression was therefore not considered to be significant for the range of ^{10}B tissue loadings studied.

The emission of a 478 keV γ-ray accompanies 93.9 per cent of $^{10}B(n,\alpha)Li^{7}$ reactions. The standard calculations did not include this γ-ray. When 1 μg ^{10}B g^{-1} of tissue was included in the phantom the 478 keV γ-ray contribution to dose was found to be negligible. The increase in dose resulting from the 478 keV γ-ray is offset by the lowering of neutron flux due to the capture in ^{10}B. Hence it is valid to ignore the contribution of this γ-ray in calculations.

The AUS module EDITAR [Robinson 1986] was used to calculate relative biological effectiveness (RBE) dose-depth data. The absorbed dose components are

(a)	neutron dose	H(n,n)H, *i.e.* proton recoil for high energy neutrons, $^{14}N(n,p)^{14}C$ for neutrons of low energy,
(b)	gamma dose	induced gammas in tissue from $^{1}H(n,\gamma)^{2}H$, reactor core gammas, induced gammas in the filter, and
(c)	boron dose	$^{10}B\ (n,\alpha)^{7}Li$

Neutron and gamma fluxes were converted to absorbed doses using ENDFB/IV kerma factors and the RBE values (2.0, 1.0 and 3.7 for the neutron, gamma and ^{10}B components of dose, respectively) of Zamenhof *et al.* [1975] were used to obtain the final RBE doses. More recent experiments by Gable *et al.* [1983] report a lower value of 2.3 for the RBE for boron capture.

Therapeutic gain was calculated as a function of depth in a phantom and used to choose the optimum filters and filter lengths for fast neutrons, thermal neutrons and gammas. Therapeutic gain was defined as the ratio of the tumour RBE dose to the maximum tissue RBE dose.

5. PHOTO-NEUTRON PRODUCTION IN D_2O

Fast neutron production by the 2.2 MeV threshold (γ,n) reaction in D_2O is ignored in calculations because of its low cross section (less than 3 mb) for the relevant energy range. Aoki and Kanda [1983], however, found that to get good agreement between calculated and measured fast and epithermal fluxes, for depths of over 60 cm in D_2O the (γ,n) reaction must be included in calculations. As HIFAR is a D_2O moderated and cooled reactor, calculations were undertaken to check the effect of the photo-neutron production on the fast and epithermal neutron fluxes. To calculate the neutron production rate from the $^{2}H(\gamma,n)^{1}H$ reaction, a transfer matrix defining production of neutrons of given energies from photons of given energies was required. Deuterium (γ,n) cross sections and the measured photo-neutron angular distribution for incident 2.72 MeV photons [Breit 1973] were used to generate a P_0 transfer matrix. The constant photo-neutron angular distribution was used because the measurements of Holland *et al.* [1981] show that it does not change greatly over the incident gamma energy range.

Calculations with and without the $^{2}H(\gamma,n)^{1}H$ reaction showed no significant flux differences along the beam tube; hence the (γ,n) reaction was not included in subsequent calculations. However, it was noted that for points within the D_2O reflector approximately 60 cm from the core and with low neutron fluxes, the photo-neutron contribution to some group fluxes was as high as 40 per cent. This supports the claim of Aoki and Kanda [1983] that for distances in D_2O which are greater than 60 cm, neutrons generated from the (γ,n) reaction become significant.

6. OPTIMUM FILTER AND GAMMA SHIELD CALCULATIONS

For a given tumour dose intensity, AlF_3 generated a slightly lower gamma dose than the other filters and was chosen for further study. A partly iterative procedure was adopted to determine the optimum length of AlF_3 filter, ^6LiF thermal neutron shield and Pb or Bi gamma shield. These thermal and γ-ray filters are placed at the beam exit to minimise the effect of small angle neutron scattering of the beam. The lengths of AlF_3, ^6LiF and Pb were each varied in turn while keeping the other two constant. Therapeutic gain curves were used to determine the optimum filter lengths for treatment of deep-seated (that is deeper than about 2.5 cm) melanomas. Except where otherwise stated, ^{10}B tumour and tissue loadings of 40 and 4 $\mu g\ g^{-1}$, respectively, were assumed. These loadings are considered to be achievable with third generation boron compounds [Soloway *et al.* 1986].

7. THERMAL NEUTRON SHIELD

Lithium fluoride was chosen because it is a thermal neutron absorber which produces practically no γ-rays. Dose depth curves for varying ^6LiF thickness (with 12 cm AlF_3 and 5 cm Pb) are given in **figure 6**; therapeutic gain curves (**figure 7**) indicate an optimum ^6LiF thickness of about 0.05 cm. For zero thickness of ^6LiF the beam is predominantly thermal. **Figure 7** shows how effective a thermal neutron beam is for treatment of tumours which are close to the surface of the skin (< 3 cm).

8. GAMMA SHIELD

The usual choice of a gamma shield for thermal neutron beams for biological purposes is bismuth, because of its low thermal capture cross section and hence low yield of induced gammas. The beam in this study, however, is largely epithermal, as the thermal component has been reduced by the ^6LiF thermal neutron shield. The capture reaction resonance integral is slightly lower for lead than for bismuth, suggesting that for an epithermal beam, a lead gamma shield could be superior. Tumour dose-depth curves and therapeutic gain curves (**figures 8** to **11**) show no discernible differences between lead and bismuth gamma shields. The optimum thickness of lead was found to be about 5 cm, with the therapeutic gain decreasing with an increase in the thickness of lead beyond this value. For a thickness of lead beyond its optimum value the epithermal neutron dose is reduced more effectively than the high energy photon dose.

9. OPTIMUM AlF_3 FILTER LENGTH

As the length of the AlF_3 filter was increased, the neutron flux spectra (**figure 12**) showed that the fast neutron flux decreased relative to the epithermal flux. The dose rate to the tumour decreased as the AlF_3 filter length was increased for constant 0.05 and 5 cm ^6LiF and Pb thicknesses, respectively (**figure 13**). Therapeutic gain curves (**figure 14**), however, indicate that there is an optimum length of filter beyond which therapeutic gain decreases slightly as the filter length increases. For an insight into the reason for this decrease, the attenuation of the various components of dose to tissue was investigated as a function of AlF_3 filter length. The neutron, gamma and ^{10}B dose rates at a depth of 3 cm in tissue as a function of AlF_3 filter length are shown in **figure 15**. It is evident that the neutron dose (approximately 75 per cent of which is fast neutron dose) attenuates more rapidly than the boron capture dose and the gamma dose attenuates less quickly. The general effect is that for AlF_3 filter lengths greater than approximately 12 cm, the boron capture dose attenuates at a similar rate to the combined neutron and gamma dose. Hence the improvement in therapeutic gain achieved by a reduction in the fast neutron dose is largely offset by a relative increase in gamma dose.

Gamma dose and therapeutic gain curves were calculated for 12 cm and 39 cm of AlF_3 (**figures 16** to **19**) with

(i) the reactor core gammas excluded,

(ii) all gammas excluded from the beam incident on the phantom model (^6LiF/Pb/tissue), and

(iii) the standard incident beam including all gammas.

From **figures 16** and **18** it can be seen that a significant part of the gamma dose is produced in the phantom model, which includes tissue as well as ^6LiF and lead. Most of these would be induced tissue gammas from the $^1H(n,\gamma)^2H$ reaction. However the bulk of the gamma dose both for 12 cm and 39 cm of AlF_3 filter is not from the induced gammas in the phantom or in the ^6LiF or lead. From **figure 16** it can be

seen that, for a short filter length, the single most significant contribution is from the core gammas. For an increased filter length **(figure 18)**, the dose component from the gammas produced in the AlF_3 becomes significant whereas that from the core becomes negligible. Calculations of the induced gamma dose from the AlF_3 filter are in fact conservative, as the 1.78 MeV gamma which follows the beta decay of ^{28}Al has not been included.

Figures 17 and **19** give an indication of the therapeutic gains which could be achieved if the gamma component of the incident beam could be reduced. Unfortunately, **figure 19** indicates that for an AlF_3 length which is sufficient to reduce the effect of the core gammas on the therapeutic gain, the induced gammas from the AlF_3 have a dramatic, deleterious effect.

10. TANGENTIAL *v.* RADIAL BEAM

For biological purposes it is generally accepted that a tangential beam is preferable to a radial beam because of its lower fast neutron and gamma components. To estimate the relative therapeutic advantage of a conceptual tangential beam, angular fluxes at the core end of 10H and at 4° and 81° to the radial direction were used to approximate as closely as possible radial and tangential beams. The tangential beam and collimator were assumed to be identical geometrically to the radial in every respect except collimator length — which, being tangential, was accordingly slightly longer. The tumour dose-depth and therapeutic gain curves for the radial and tangential beams, with a zero length of AlF_3 filter, are given in **figures 20** and **21**. The optimum radial beam, produced by the use of 12 cm AlF_3, 0.05 cm ^6LiF and 5 cm Pb filters is also shown for comparison. The therapeutic advantage of a tangential beam is obvious even to depths of 7 or 8 cm in tissue while the penalty in dose is similar to that incurred by the use of a 12 cm AlF_3 filter. Components of the RBE dose as a function of depth in phantom tissue are given in **table 4** for the optimum radial, radial and tangential beams for a ^{10}B concentration of 1 μg ^{10}B g^{-1} tissue. The tangential horizontal D_2O facility (2TAN) just below the core in HIFAR is of small cross-section (3.81 x 10.8 cm) and has not been considered in this study.

11. THERAPEUTIC GAIN VARIATION WITH BORON CONCENTRATION

Therapeutic gain as a function of ^{10}B concentration was calculated for the optimum beam for several ^{10}B tumour-to-tissue ratios. Calculations were for depths of 1.75 and 7.25 cm and in tissue for a single field **(figure 22)** as well as at a depth of 7.25 cm for a 15 cm slab exposed to opposing fields **(figure 23)**. The opposing neutron field results for a 15 cm thick phantom slab irradiated from opposite sides were derived from the 30 cm phantom calculations, and hence will be slightly in error at the edges. From the curves it can be seen that useful increases in therapeutic gain can be achieved by increases in the absolute and relative ^{10}B tumour concentrations. Tumour dose and therapeutic gain are presented in **figures 24** and **25** as a function of depth in a phantom for a range of ^{10}B loadings and a ^{10}B tumour-to-tissue ratio of 10.

Figures 26 and **27** show tumour dose and therapeutic gain curves for various ^{10}B loadings for a 15 cm tissue slab exposed to beams from opposite directions. From these it can be seen that for an opposing field both the dose and therapeutic gain at the centre of the tissue slab are approximately double relative to the single field.

12. CONCLUSIONS

Calculations were undertaken to examine the feasibility of developing an epithermal beam in the 10H horizontal facility in HIFAR, suitable for treatment of deep-seated metastatic melanoma. Filters considered likely to provide sufficient beam intensity were Al, Al/S and AlF_3. The optimum neutron and gamma filters and their lengths were determined by maximising therapeutic gain (tumour RBE dose/maximum tissue RBE dose) in a phantom at depths greater than about 3 cm.

A survey of calculated therapeutic gains and dose rates with varying filter lengths, is presented. The optimum filter arrangement is found to be 12 cm AlF_3, 0.05 cm ^6LiF and 5 cm Pb. Nevertheless, the advantage of using a 12 cm AlF_3 rather than no AlF_3 filter is questionable, as the tumour dose rate is approximately halved for a relatively small improvement in therapeutic gain.

Calculations of dose characteristics confirm the superiority of a tangential beam over a radial beam. This gives much larger improvements in therapeutic gain than the use of an AlF_3 filter in a radial beam. Useful increases in therapeutic gain can also be achieved by increasing absolute or relative ^{10}B tumour

concentrations. Possible beams in HIFAR which are tangential to the core are the 2TAN facility and the vertical D_2O facilities, but these are all smaller than 10H.

The disappointing results from an AlF_3 filter arise because most of the advantage in therapeutic gain achieved by the attenuation of the fast neutron dose is counteracted by an increase in the gamma dose. The gammas induced in Al are high in energy and cannot be attenuated by lead or bismuth without further detriment to the neutron beam.

An important finding of the study is that in estimating the effect of various neutron and gamma filters on the dose to tissue, the total effect of the filters must be considered; that is, the effect of each filter on both the neutron dose and gamma dose must be included. Other studies, such as the design study of an epithermal beam by Oka *et al.* [1981] have assumed that the problem can be treated in several unrelated parts. In such studies various filters and filter geometries have been examined to determine their effectiveness in reducing the fast neutron dose of the beam, while ignoring their effect on the induced gamma dose. Similarly, gamma shields have been chosen to reduce the gamma dose to an arbitrarily low level without considering the effect they might have on the neutron beam spectrum and intensity. The present studies show conclusively that any assessment of a filter arrangement based on the effect of individual components on either the neutron dose or gamma dose in isolation is inadequate and likely to lead to erroneous conclusions.

13. ACKNOWLEDGEMENTS

The assistance of G.S. Robinson and B.J. McGregor in the use of codes and development of models is gratefully acknowledged. Thanks are due also to J.W. Connolly and B.J. Allen for helpful discussions.

14. REFERENCES

Allen, B.J., Brown, J.K., Harrington, B., Izard, B., Linklater, H., Maddalena, D.J., McNeill, J., McGregor, B.J., Mountford, M.H., Snowdon, G.M., Wilson, D.J., Wilson, J.G., Parsons, D., Moore, D., Tamat, S., Hersey, P. [1986] - *Neutron Capture Therapy, Second Int. Symp. on Neutron Capture Therapy*, Oct. 18-20, 1985, Tokyo. ed. H. Hatanaka, Nishimura, Niigata, p.258.

Aoki, K., Kanda, K. [1983] - Effect of (γ,n) reactions of heavy water moderator on beam quality in biomedical irradiation facility. *J. Nucl. Sci. Technol.*, 20(10)812.

Breit, G. [1973] - Photodisintegration of the deuteron theory. *Int. Conf. on Photonuclear Reactions*, March 26-30. CONF-750301.

Constantine, G., Baker, L.J., Taylor, N.P. [1986] - Improved methods for the generation of 24.5 keV neutron beams with possible application to boron neutron capture therapy. *Nucl. Instrum. Methods Phys. Res.*, A250:565.

Engle, W.W. [1967] - A users' manual for ANISN. K-1693.

Ford, W.E., Santoro, R.T., Roussin, R.W., Plaster, D.M. [1976] - Modification number one to the coupled 100 n-21 cross-section library for EPR calculations. ORNL-TM-5249.

Gable, D., Fairchild, R.G., Larsson, B., Drescher, K., Rowe, W.R. [1983] - The biological effect of the $^{10}B(n,\alpha)^7Li$ reactions and its simulation by MONTE CARLO calculations. *Proc. First Int. Symp. on Neutron Capture Therapy.* BNL-51730.

Garber, D. [1975] - ENDF/B summary documentation. BNL-17541.

Harrington, B.V. [1983] - Neutronic models for the HIFAR reactor. AAEC/E571.

Hehn, G. [1983] - PWR shielding benchmark. NEACRP-L-264.

Holland, R.E., Holt, R.J., Jackson, H.E., McKeown, R.D., Specht, J.R., Stephenson, K.E. [1981] - Physics Division Annual Review, 1 April 1980 - 31 March 1981. Argonne National Lab. ANL-81-79, p.108.

Jaeger, R.G., Blizard, E.P., Chilton, A.B., Grotenhuis, M., Honig, A., Jaeger, Th.A. [1968] - Engineering Compendium on Radiation Shielding. Vol. I. Springer-Verlag, New York, p.507.

McGregor, B.J., Allen, B.J. [1983] - Filtered beam dose distributions for boron neutron capture therapy of brain tumours. *Proc. First Int. Symp. on Neutron Capture Therapy.* BNL-51730, p.14.

Mill, A.J., Harvey, J.R. [1978] - Intermediate energy neutron production - A survey of existing techniques. EUR 6107 EN.

Noonan, D.J., Russell, J.L., Jnr. [1983] - Biological studies of an epithermal beam for NCT with $Na_2B_{12}H_{11}SH$. *Proc. First Int. Symp. on Neutron Capture Therapy.* BNL-51730, p.315.

Oka, Y., Nanagisawa, I., An, S. [1981] - A design study of the neutron irradiation facility for boron neutron capture therapy. *Nucl. Technol.*, 55:642.

Pollard, J.P. [1974] - AUS module POW - A general purpose 0, 1 and 2D multigroup neutron diffusion code including feed back-free kinetics. AAEC/E269.

Rhoades, W.A., Mynatt, F.R. [1973] - The DOT 3.5 two-dimensional discrete ordinates transport code. ORNL-TM-4280.

Robinson, G.S. [1975] - AUS - The Australian modular scheme for reactor neutronics computations. AAEC/E369.

Robinson, G.S. [1977] - AUS module MIRANDA - a data preparation code based on multiregion resonance theory. AAEC/E410.

Robinson, G.S. [1986] - EDITAR - A module for reaction rate editing and cross-section averaging within the AUS neutronics code system. AAEC/E621.

Soloway, A.H., Alan, F., Barth, R.F. [1986] - Future boronated molecules for neutron capture therapy. *Workshop on Neutron Capture Therapy.* BNL-51994, p.162.

Zamenhof, R.G., Murray, B.W., Brownell, G.L., Wellum, G.R., Tolpin, E.L. [1975] - Boron neutron capture therapy for the treatment of cerebral gliomas. *Med. Phys.*, 2:47.

TABLE 1
NEUTRON GROUP BOUNDARIES

Group	Energy(eV)	Group	Energy(eV)
1	1.54883E+07	36	4.30742E+03
2	8.29029E+06	37	3.35463E+03
3	6.06531E+06	38	2.61259E+03
4	5.02832E+06	39	2.03468E+03
5	4.16862E+06	40	1.58461E+03
6	3.24652E+06	41	1.23410E+03
7	2.69146E+06	42	9.61116E+02
8	2.23130E+06	43	7.48518E+02
9	1.84981E+06	44	5.82947E+02
10	1.53355E+06	45	4.53999E+02
11	1.19433E+06	46	3.53575E+02
12	9.90134E+05	47	2.75364E+02
13	8.20850E+05	48	2.14454E+02
14	6.80509E+05	49	1.67017E+02
15	5.64161E+05	50	1.30073E+02
16	4.39369E+05	51	1.01301E+02
17	3.64250E+05	52	7.88932E+01
18	3.01974E+05	53	6.14421E+01
19	2.50345E+05	54	4.78512E+01
20	2.07543E+05	55	3.72665E+01
21	1.61635E+05	56	2.90232E+01
22	1.42642E+05	57	2.26033E+01
23	1.11090E+05	58	1.76035E+01
24	8.65169E+04	59	1.37096E+01
25	6.73794E+04	60	1.06770E+01
26	5.24752E+04	61	8.31529E+00
27	4.08677E+04	62	6.47595E+00
28	3.18278E+04	63	5.04348E+00
29	2.47875E+04	64	3.92786E+00
30	1.93045E+04	65	3.05902E+00
31	1.50344E+04	66	2.26618E+00
32	1.17088E+04	67	1.85539E+00
33	9.11882E+03	68	4.13994E-01
34	7.10174E+03		1.02619E-05
35	5.53084E+03		

TABLE 2
GAMMA GROUP BOUNDARIES

Group	Lower Gamma Energy (MeV)
1	10.0
2	8.0
3	7.0
4	6.0
5	5.0
6	4.0
7	3.0
8	2.0
9	1.0
10	0.4
11	0.1
12	0.01

TABLE 3
PHANTOM TISSUE COMPOSITION USED IN THESE STUDIES

Element	wt%
O	71.39
C	14.89
H	10.00
N	3.47
Cl	0.10
Na	0.15

Density = 1.00 g cm^{-3}

TABLE 4
RBE DOSE-DEPTH DISTRIBUTIONS IN PHANTOM TISSUE
(rem s^{-1}) FOR 1 μg ^{10}B g^{-1} TISSUE

		Optimum Beam			Radial Beam			Tangential Beam		
Depth	RBE	1.0	2.0	3.7	1.0	2.0	3.7	1.0	2.0	3.7
(cm)	Component	γ	p	α,^{7}Li	γ	p	α,^{7}Li	γ	p	α,^{7}Li
0-.5		0.110	0.144	0.0116	0.239	0.577	0.0225	0.0427	0.142	0.0140
.5-1.0		0.109	0.129	0.0123	0.237	0.511	0.0254	0.0462	0.124	0.0154
1.5-2.0		0.103	0.104	0.0113	0.225	0.409	0.0253	0.0478	0.096	0.0148
2.5-3.0		0.094	0.083	0.0094	0.208	0.326	0.0222	0.0458	0.074	0.0126
3.5-4.0		0.085	0.066	0.0073	0.189	0.259	0.0180	0.0418	0.056	0.0100
4.5-5.0		0.076	0.052	0.0055	0.169	0.206	0.0140	0.0370	0.043	0.0076
5.5-6.0		0.068	0.041	0.0040	0.151	0.163	0.0105	0.0321	0.032	0.0056
6.5-7.0		0.060	0.032	0.0029	0.133	0.129	0.0077	0.0274	0.024	0.0040
7.5-8.0		0.053	0.025	0.0020	0.118	0.102	0.0056	0.0233	0.018	0.0028
8.5-9.0		0.047	0.020	0.0014	0.104	0.081	0.0040	0.0197	0.014	0.0019
9.5-10.0		0.042	0.016	0.0010	0.092	0.064	0.0029	0.0167	0.010	0.0013
11.5-12.0		0.033	0.010	0.0005	0.071	0.040	0.0015	0.0120	0.006	0.0006
14.5-15.0		0.024	0.005	0.0002	0.050	0.020	0.0006	0.0074	0.003	0.0002

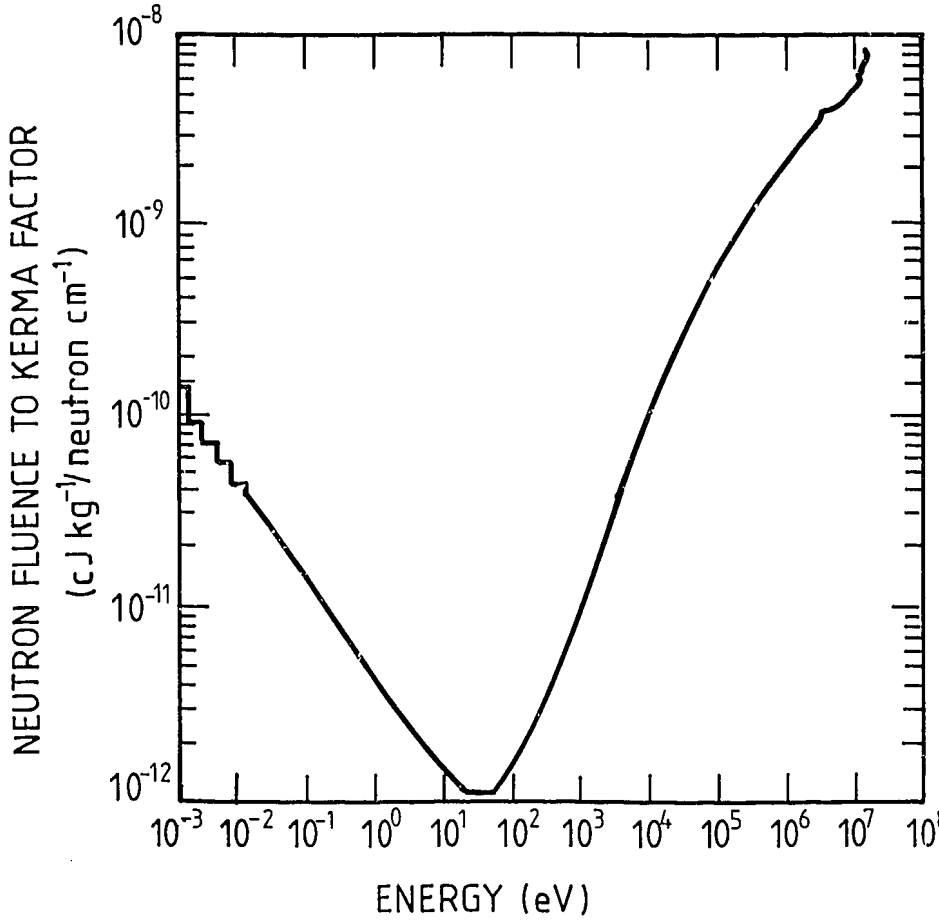

Figure 1 Neutron fluence to kerma factors from ENDFB-IV data for phantom tissue with the composition of **table 3**

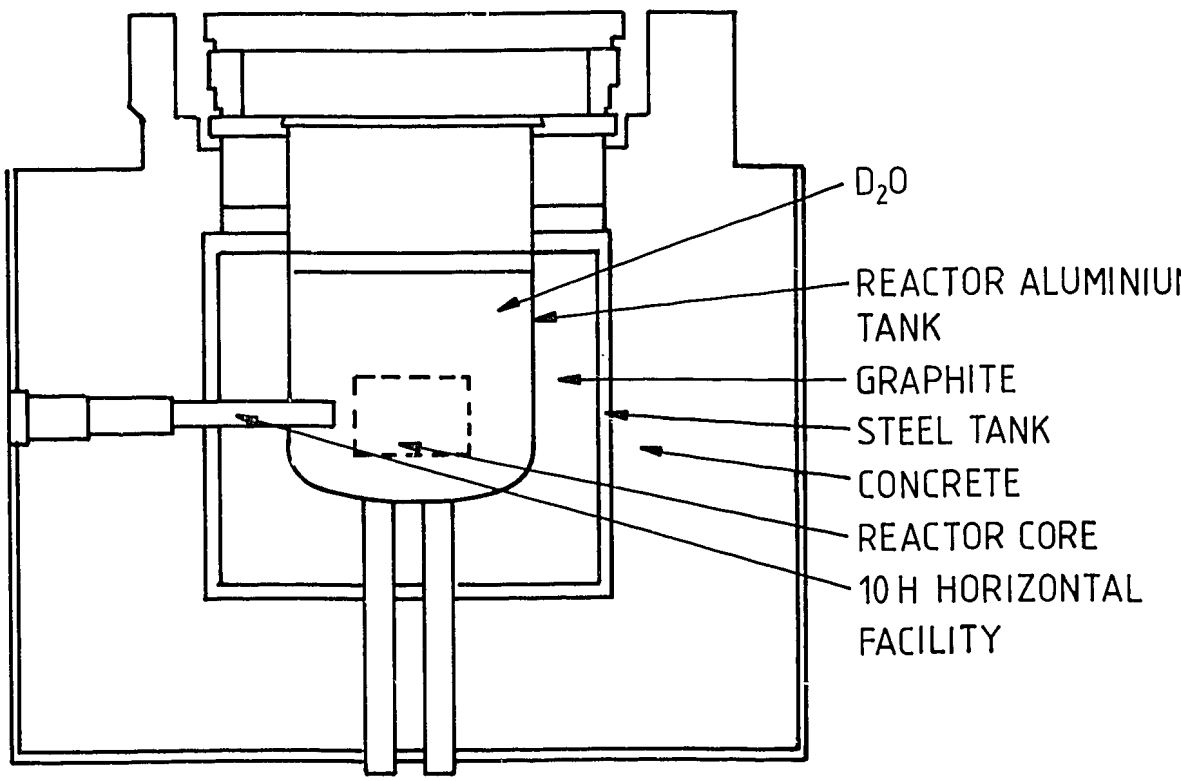

Figure 2 A section through the reactor HIFAR

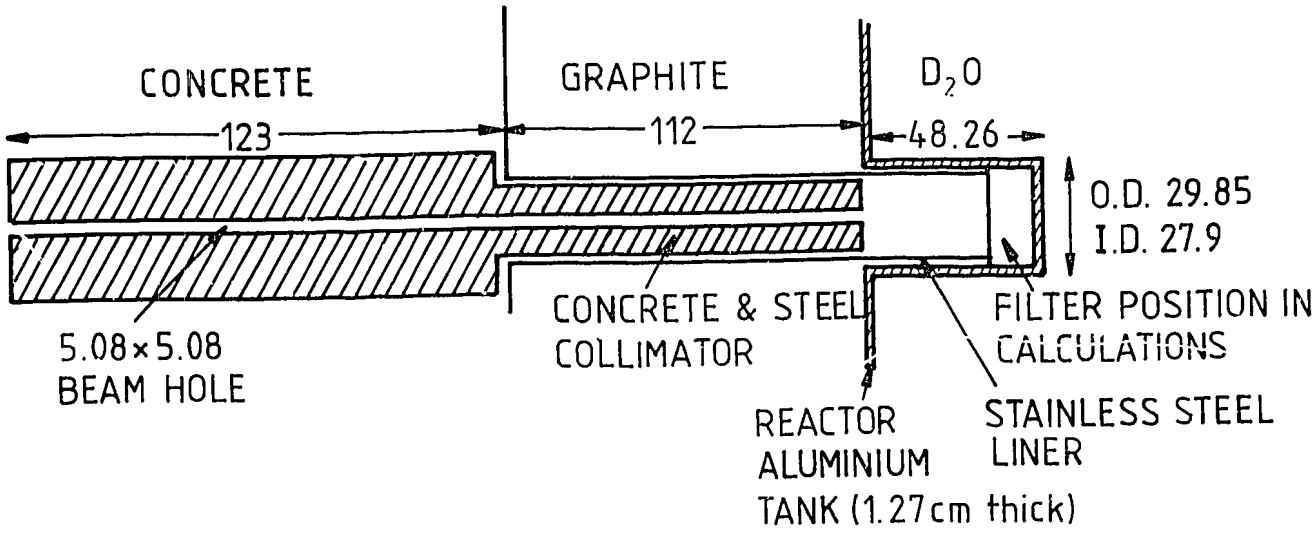

Figure 3 The 10H horizontal facility

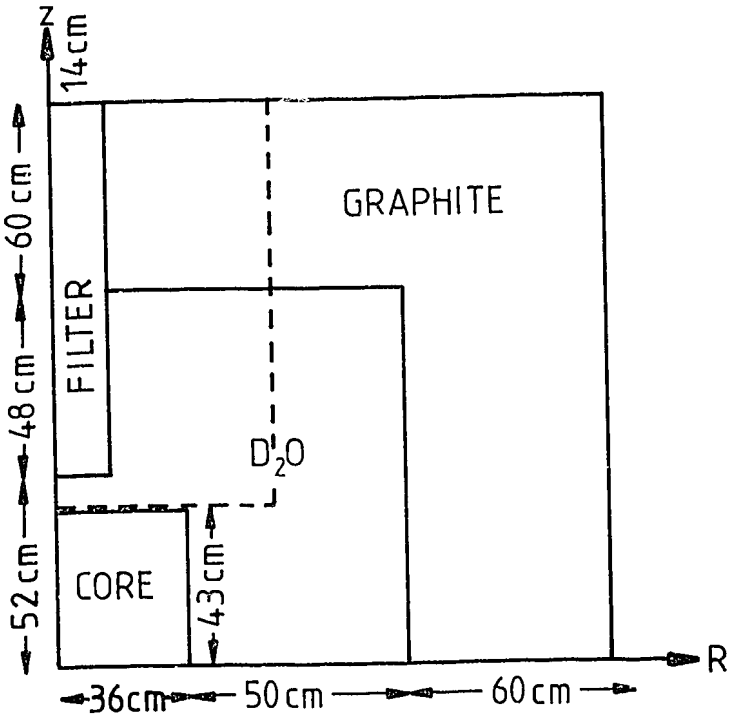

Figure 4 HIFAR model used for beam calculations

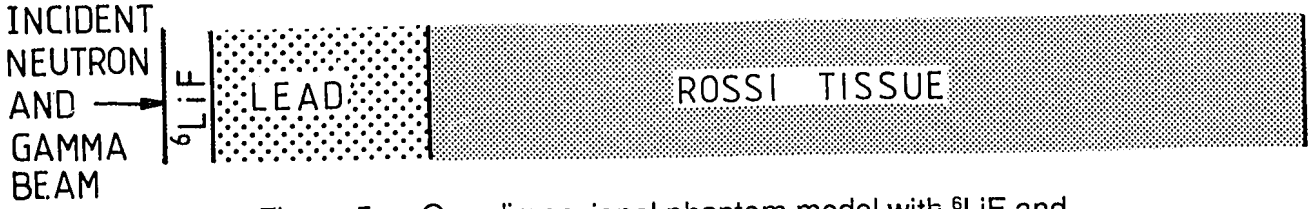

Figure 5 One-dimensional phantom model with ^6LiF and Pb shields

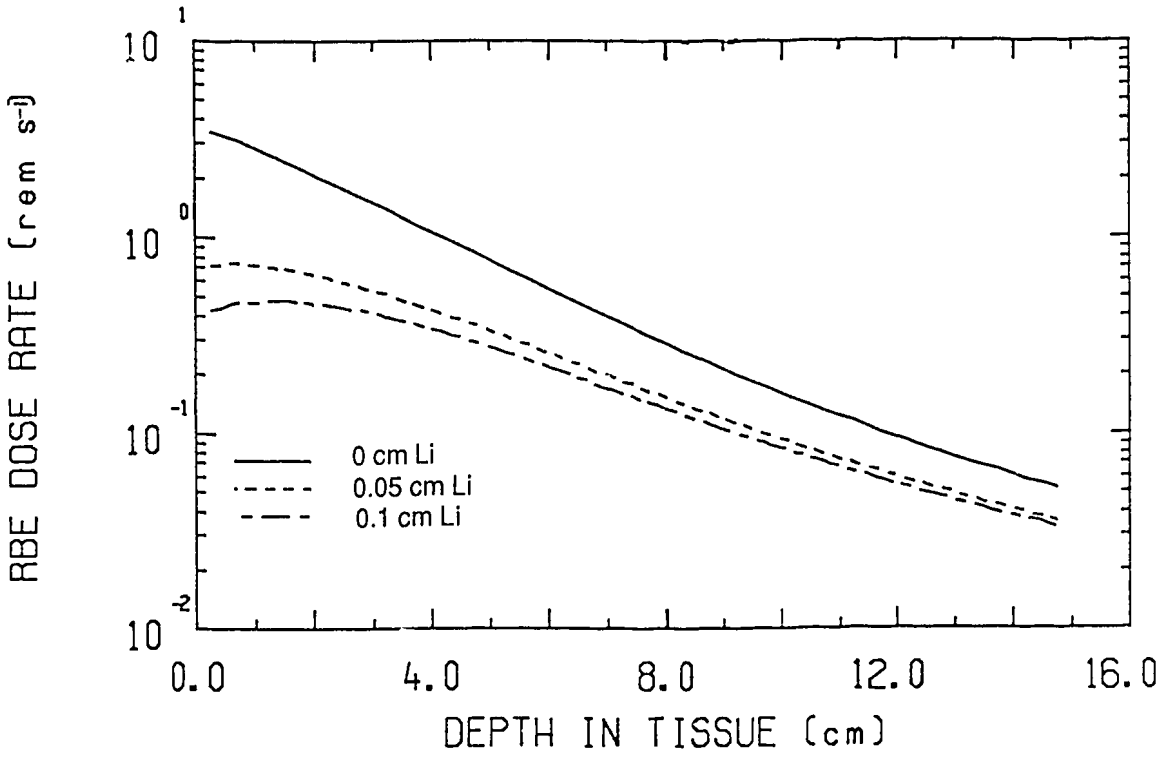

Figure 6 Tumour dose-depth curves for various ^{6}LiF lengths (40/4 μg g^{-1} ^{10}B tumour/tissue loading, 12 cm AlF_3, 5 cm Pb)

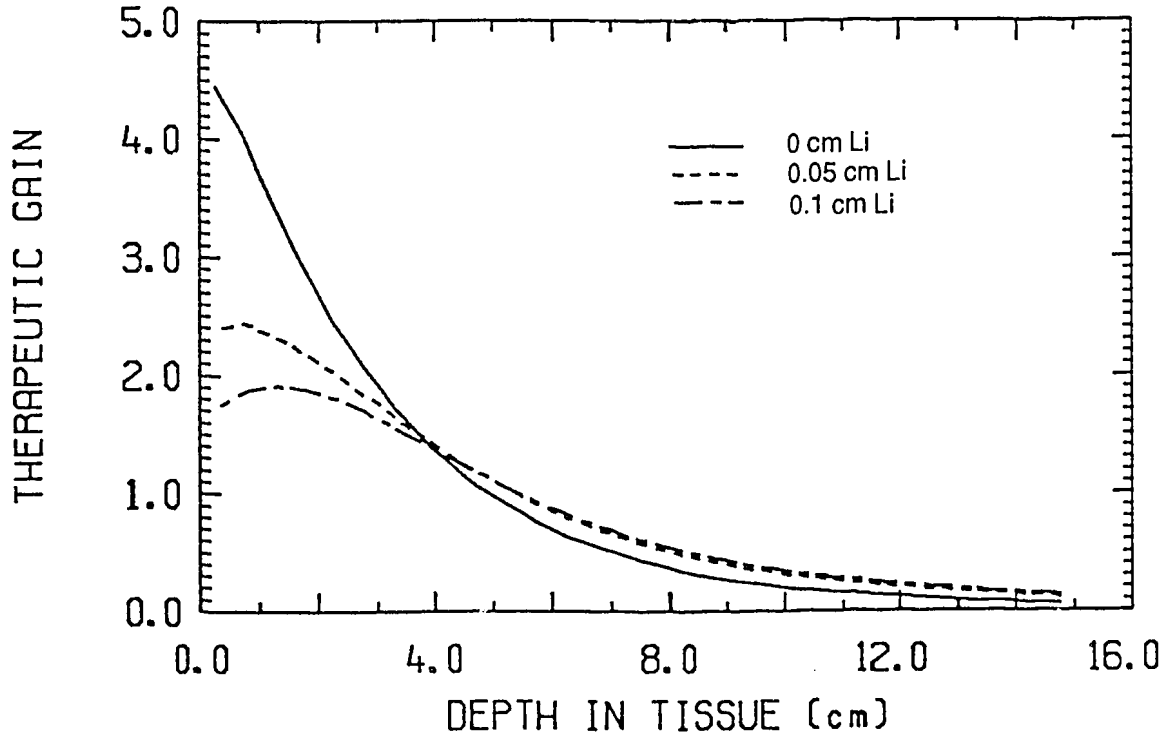

Figure 7 Therapeutic gain curves for various ^{6}LiF lengths (40/4 μg g^{-1} ^{10}B tumour/tissue loading, 12 cm AlF_3, 5 cm Pb)

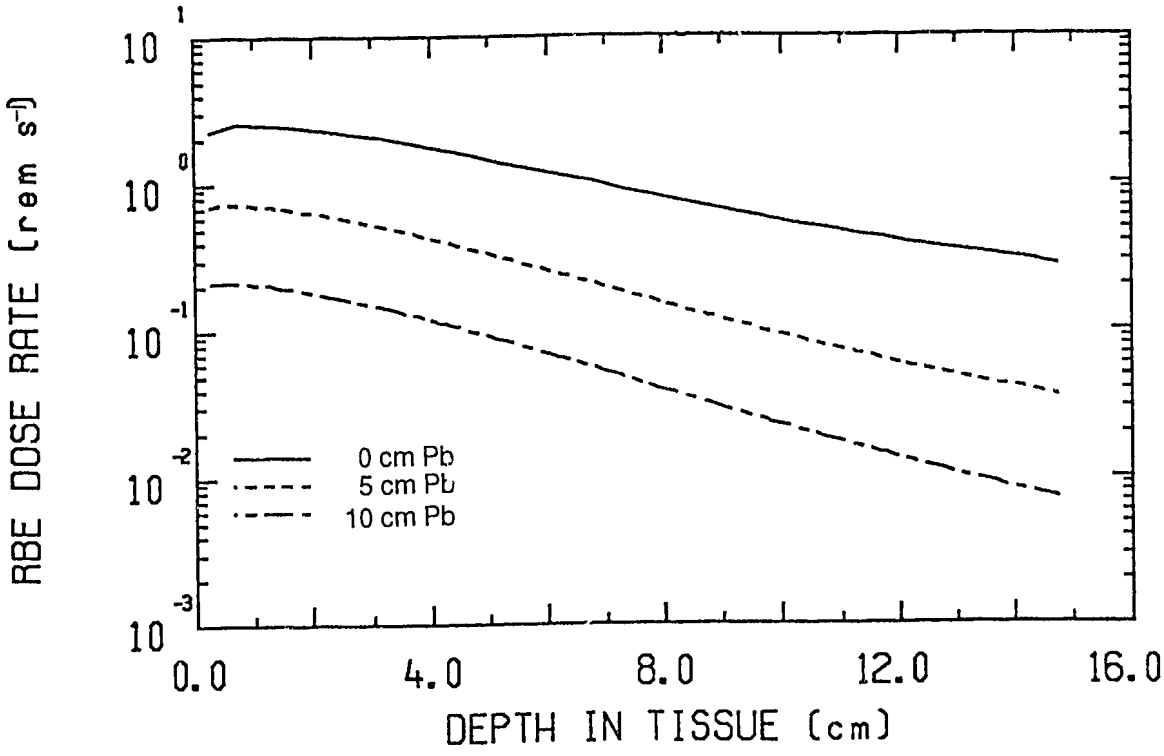

Figure 8 Tumour dose-depth curves for various Pb lengths (40/4 μg g^{-1} ^{10}B tumour/tissue loading, 12 cm AlF_3, 0.05 cm ^6LiF)

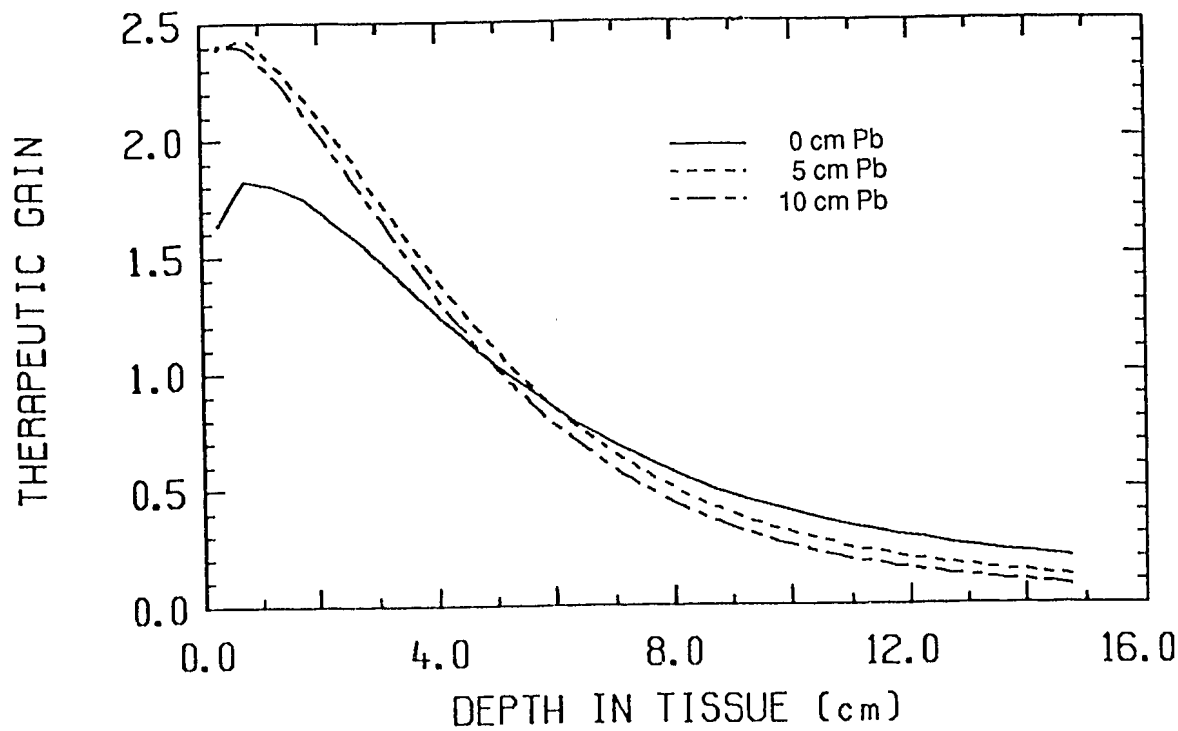

Figure 9 Therapeutic gain curves for various Pb lengths (40/4 μg g^{-1} ^{10}B tumour/tissue loading, 12 cm AlF_3, 0.05 cm ^6LiF)

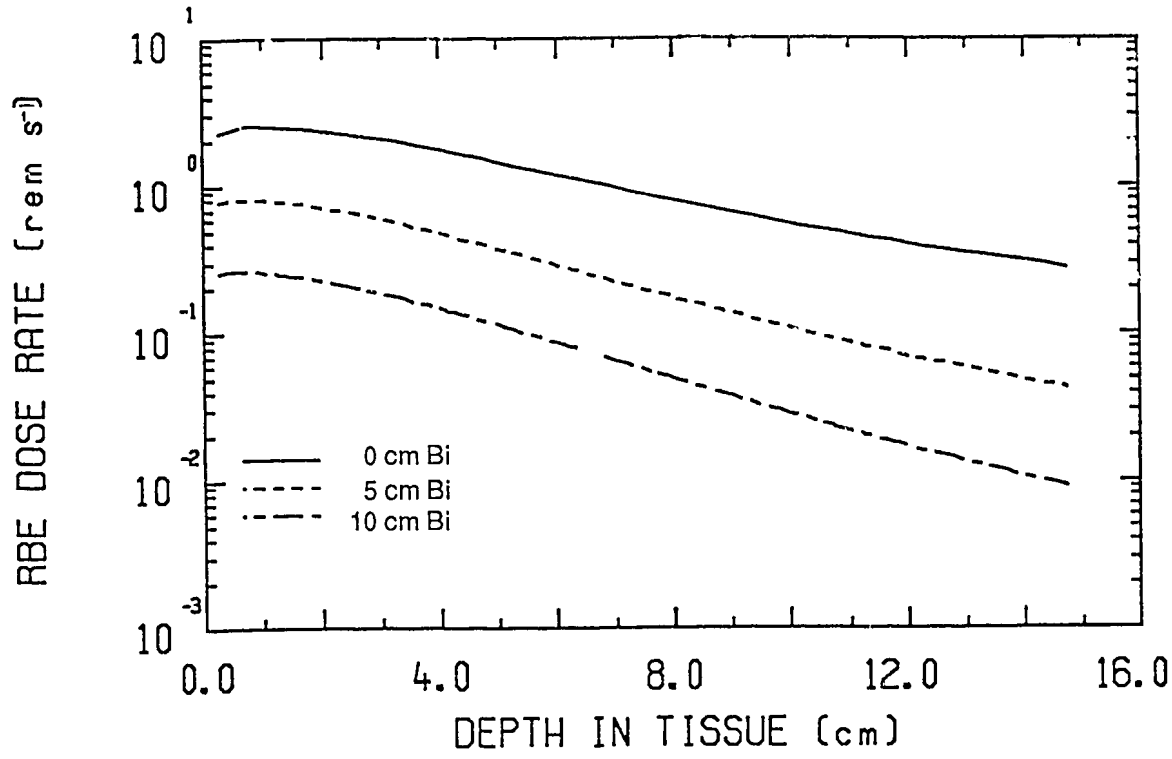

Figure 10 Tumour dose-depth curves for various Bi lengths (40/4 μg g^{-1} ^{10}B tumour/tissue loading, 12 cm AlF_3, 0.05 cm ^6LiF)

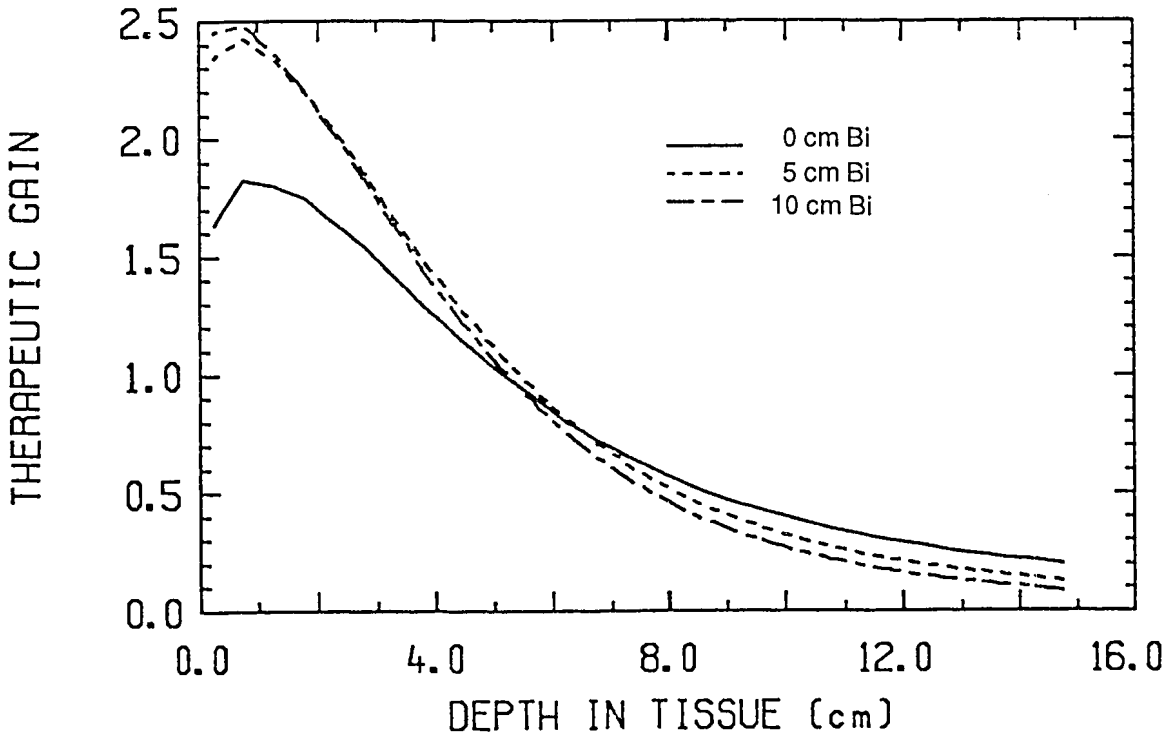

Figure 11 Therapeutic gain curves for various Bi lengths (40/4 μg g^{-1} ^{10}B tumour/tissue loading, 12 cm AlF_3, 0.05 cm ^6LiF)

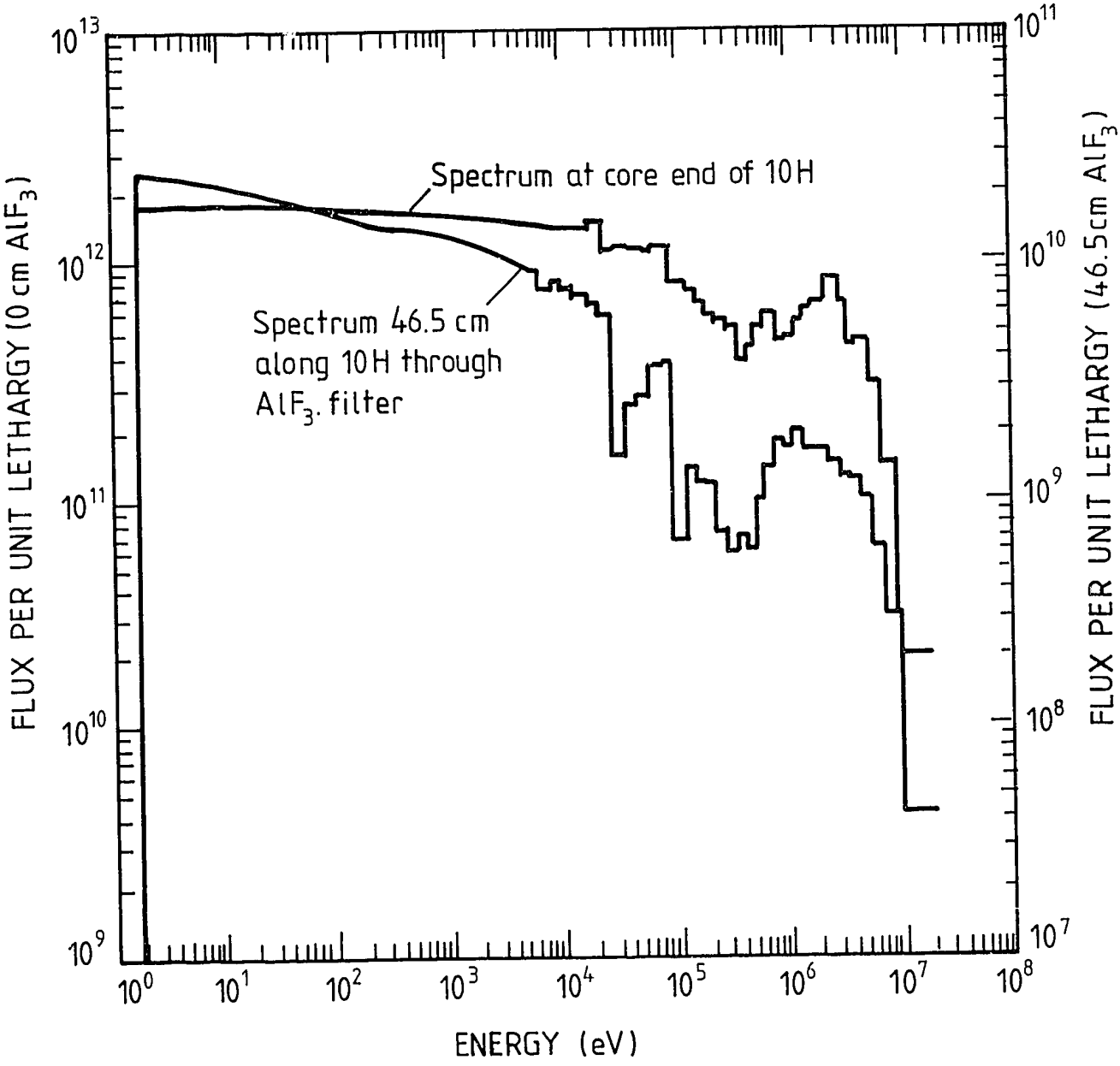

Figure 12 Shift in neutron flux spectrum through an AlF_3 filter

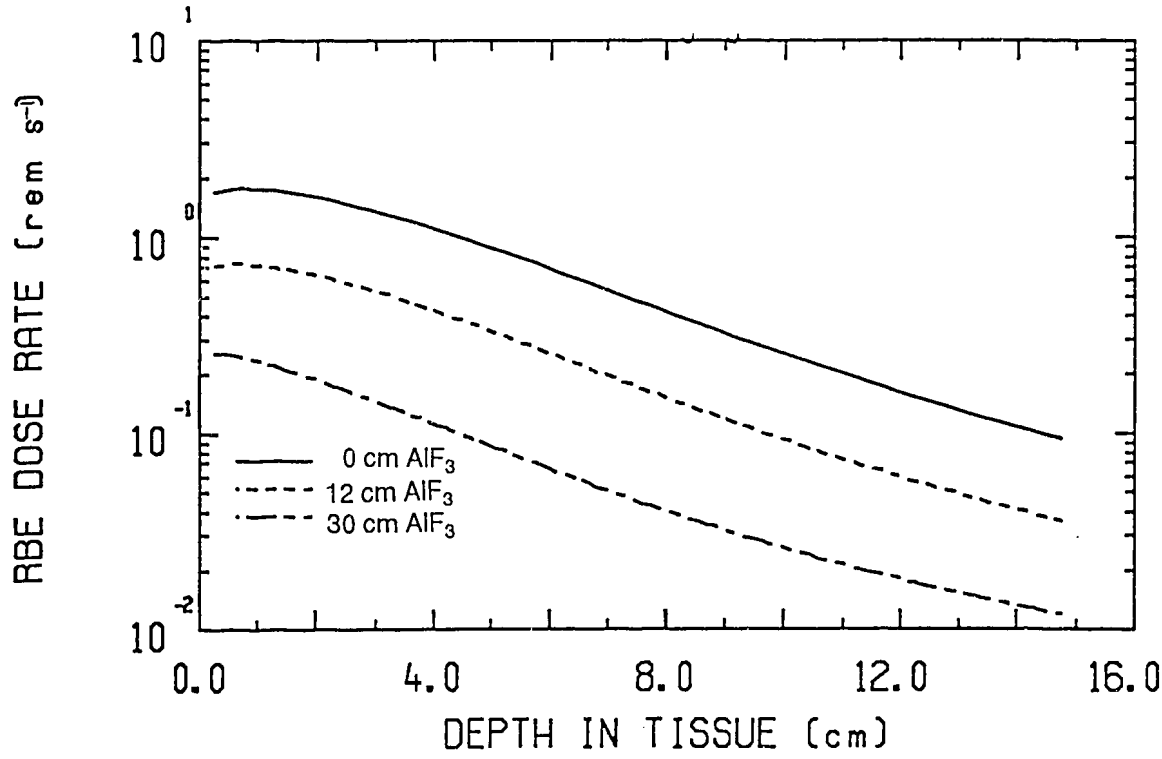

Figure 13 Tumour dose-depth curves for varying AlF_3 filter lengths (40/4 μg g^{-1} ^{10}B tumour/tissue loading, 5 cm Pb, 0.05 cm ^6LiF)

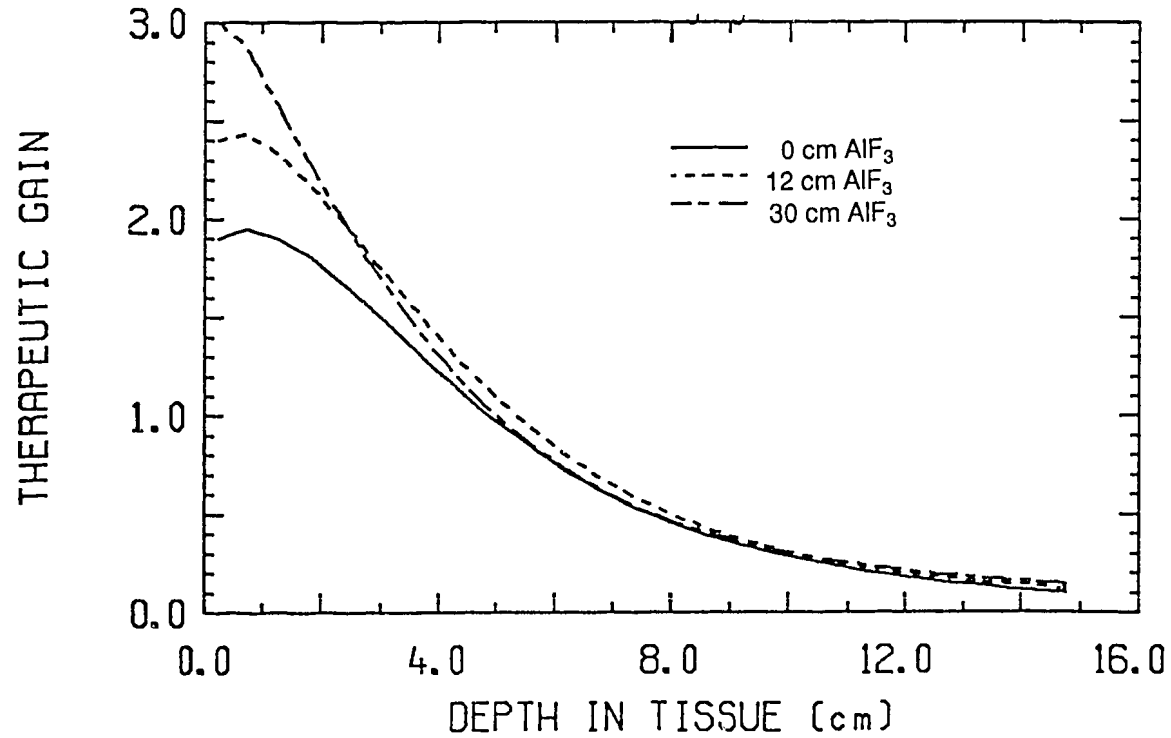

Figure 14 Therapeutic gain curves for varying AlF_3 filter lengths (40/4 μg g^{-1} ^{10}B tumour/tissue loading, 5 cm Pb, 0.05 cm ^6LiF)

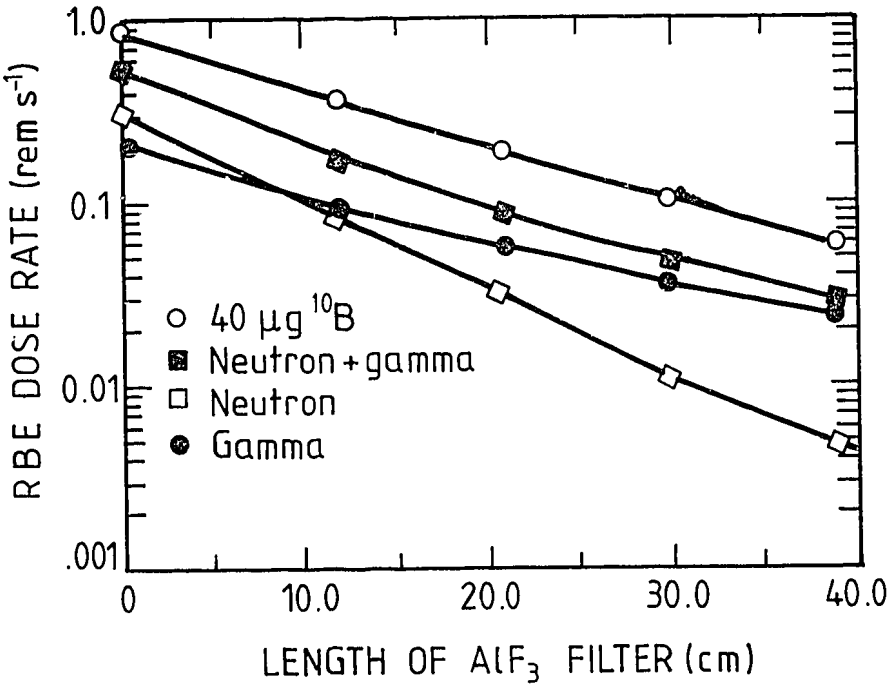

Figure 15 Components of dose as a function of AlF_3 filter length at a depth of 3 cm in phantom (5 cm Pb, 0.05 cm ^{6}LiF)

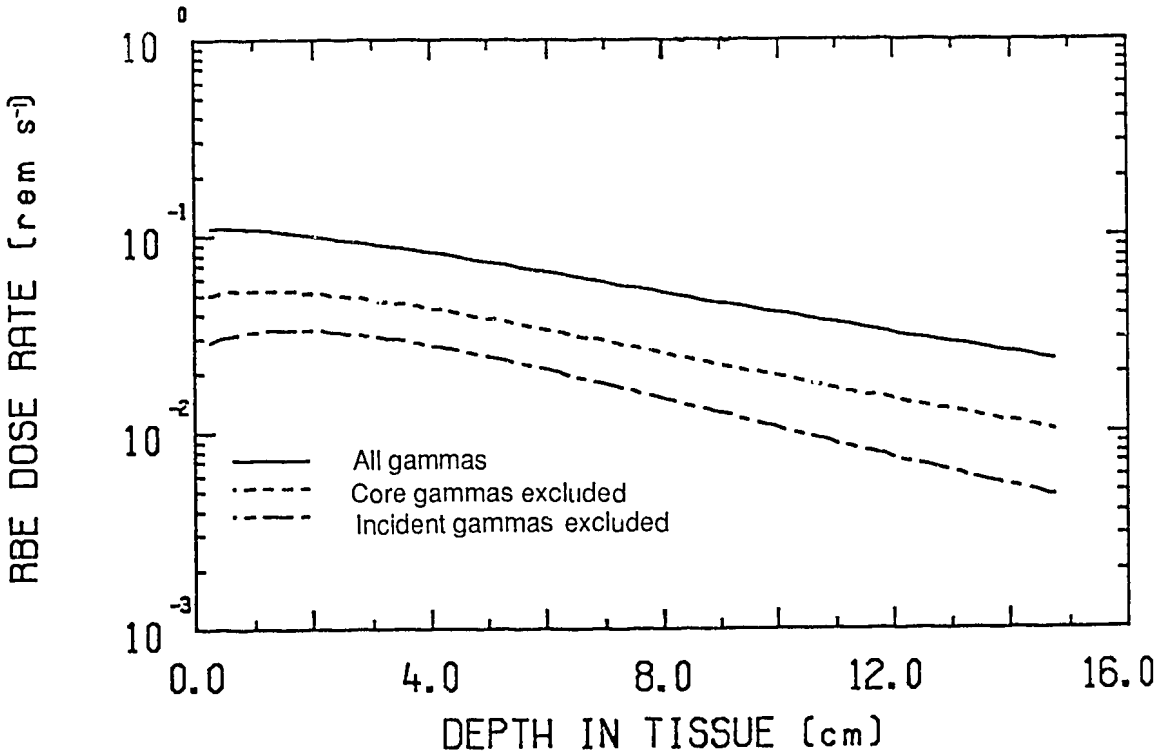

Figure 16 Gamma dose-depth curves for 12 cm AlF_3 (5 cm Pb, 0.05 cm ^6LiF)

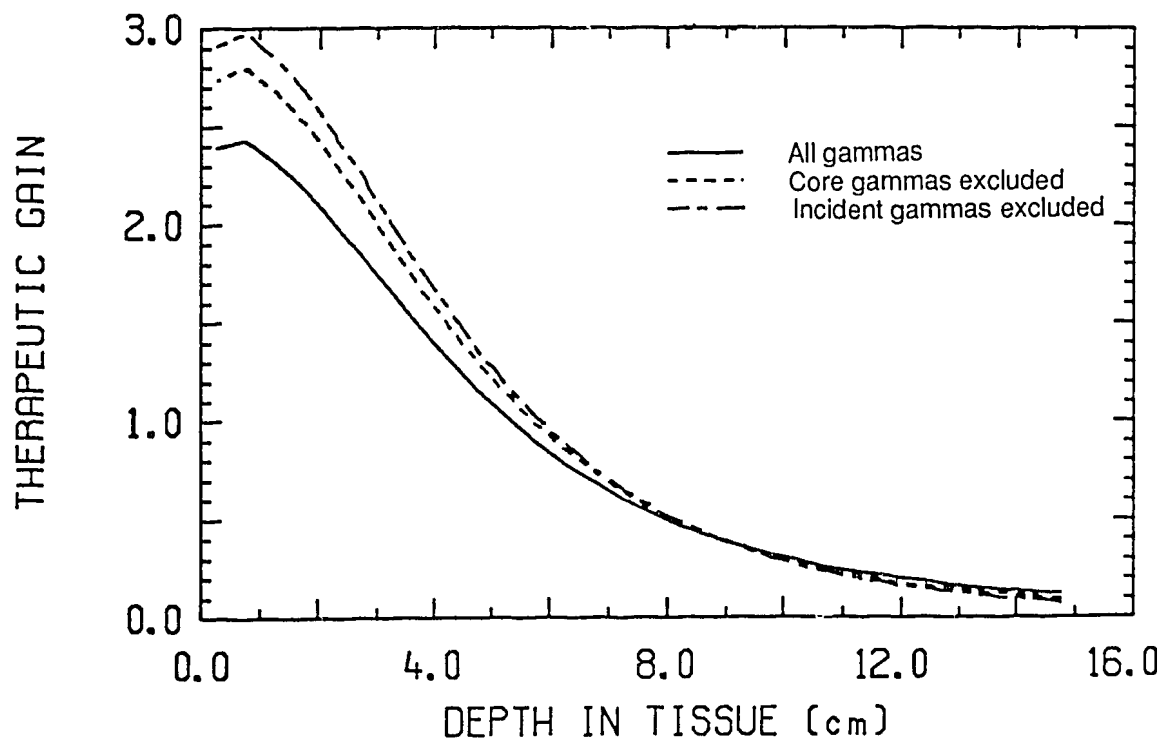

Figure 17 Therapeutic gain curves for 12 cm AlF_3 with various gamma components excluded (40/4 μg g^{-1} ^{10}B tumour/tissue loading, 5 cm Pb, 0.05 cm ^6LiF)

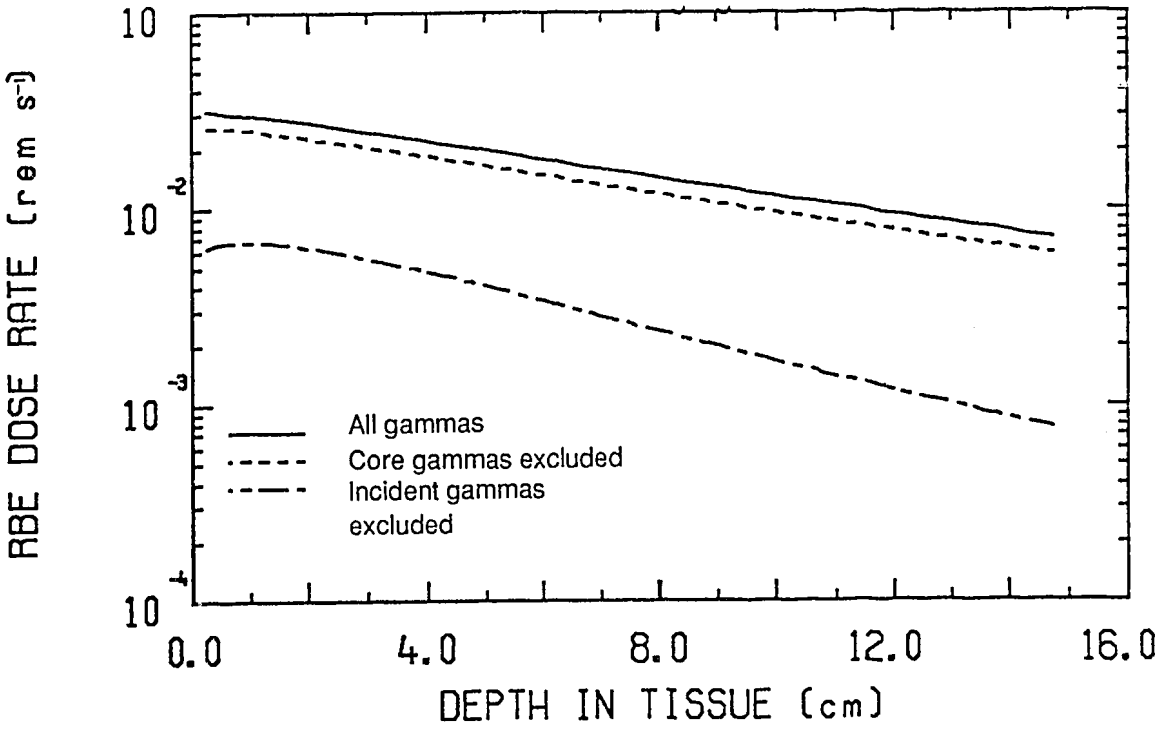

Figure 18 Gamma dose-depth curves for 39 cm AlF_3 (5 cm Pb, 0.05 cm ^6LiF)

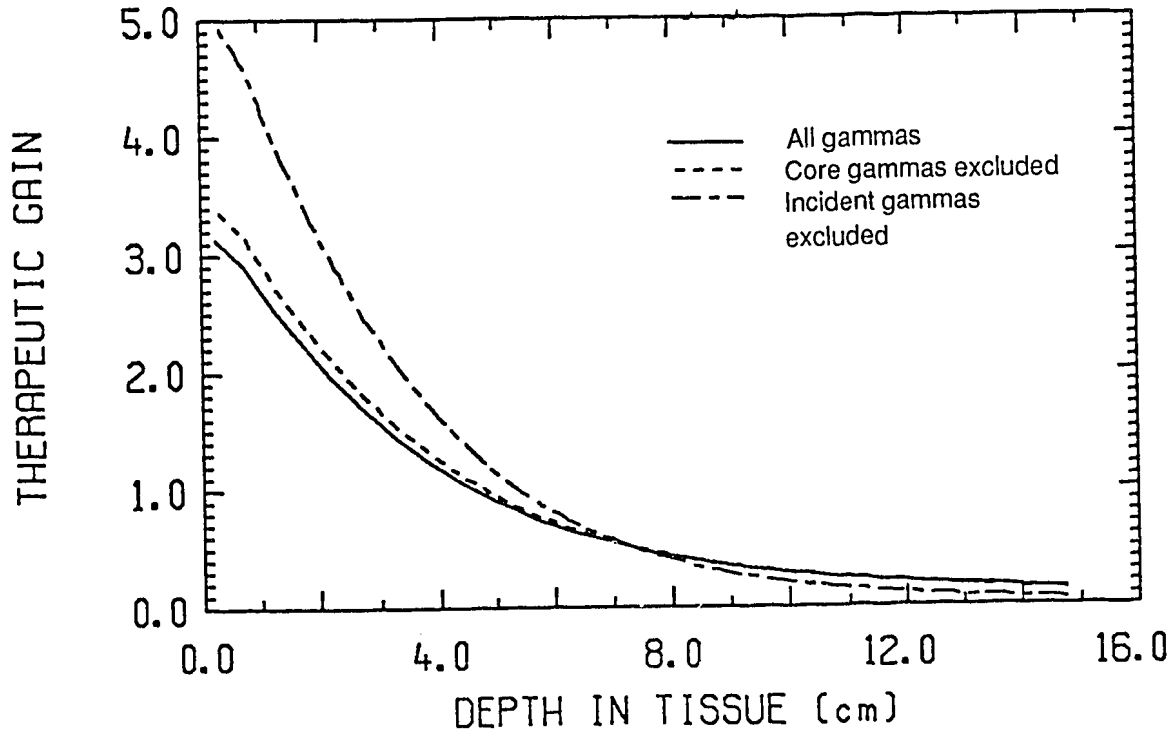

Figure 19 Therapeutic gain curves for 39 cm AlF_3 with various gamma components excluded (40/4 μg g^{-1} ^{10}B tumour/tissue loading, 5 cm Pb, 0.05 cm ^6LiF)

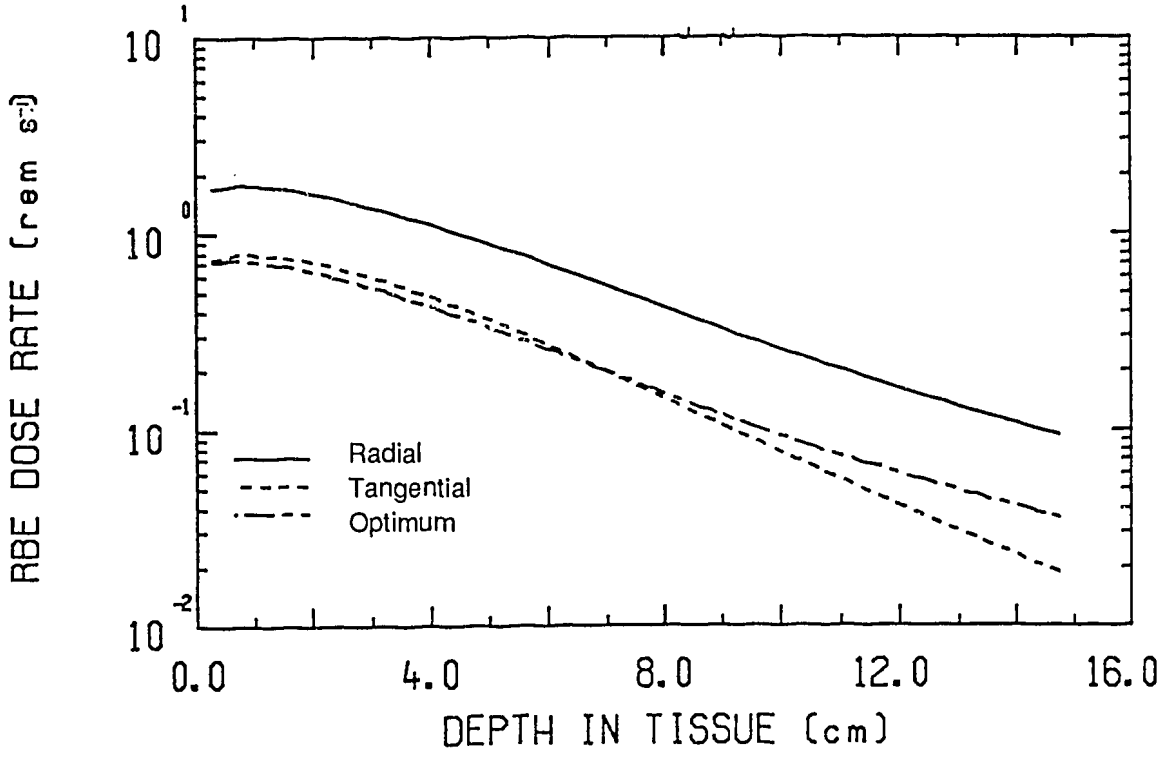

Figure 20 Tumour dose-depth curves for tangential *v.* radial beams (40/4 μg g^{-1} ^{10}B tumour/tissue loading, 5 cm Pb, 0.05 cm ^{6}LiF)

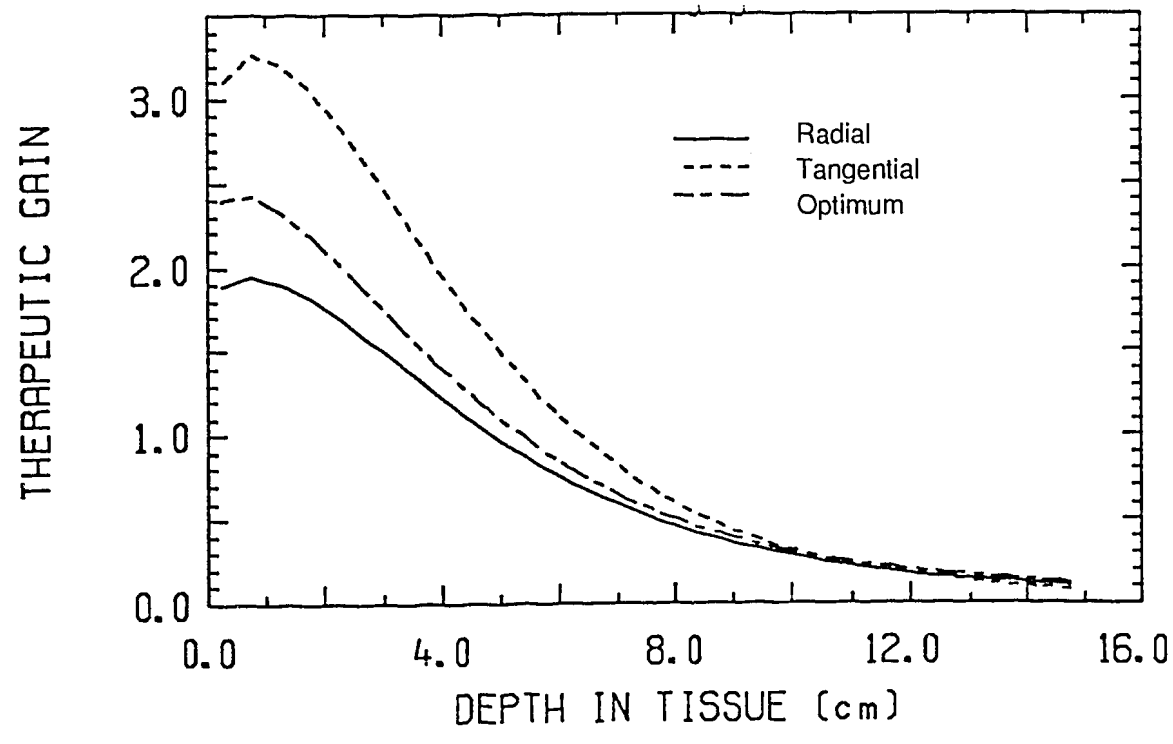

Figure 21 Therapeutic gain curves for tangential *v.* radial beams (40/4 μg g^{-1} ^{10}B tumour/tissue loading, 5 cm Pb, 0.05 cm ^{6}LiF)

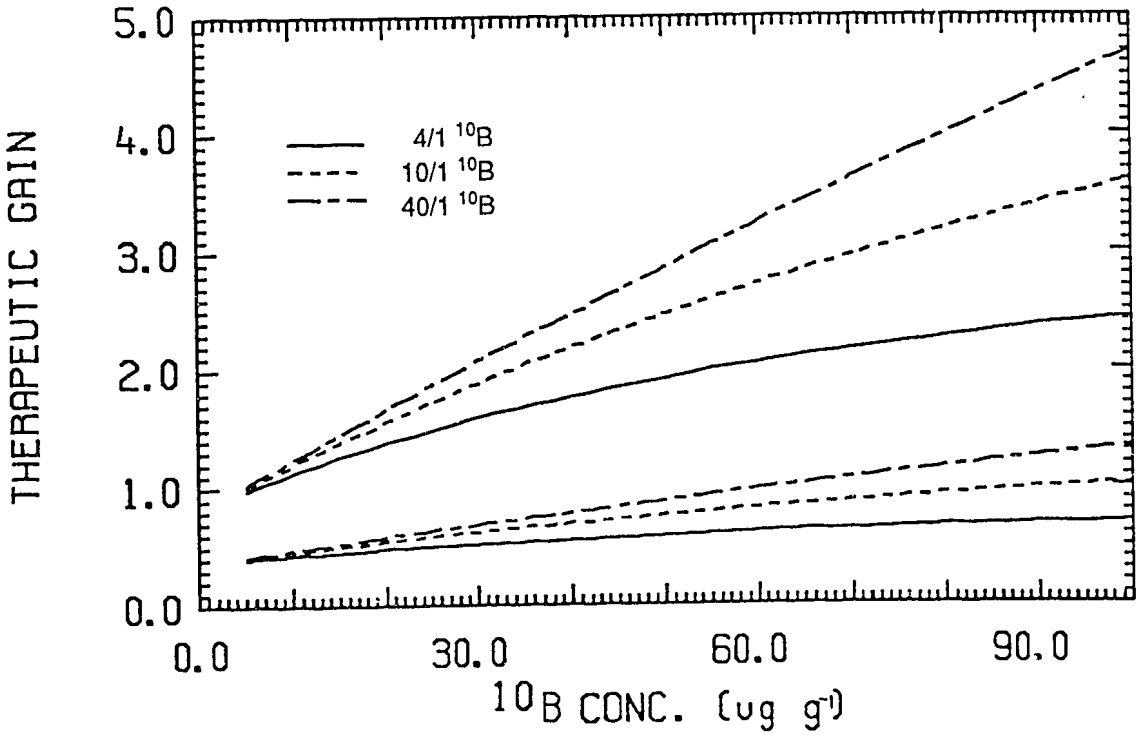

Figure 22 Therapeutic gain *v.* ^{10}B concentration for a single field at 1.75 cm and 7.25 cm depths (12 cm AlF_3, 0.05 cm ^{6}LiF, 5 cm Pb)

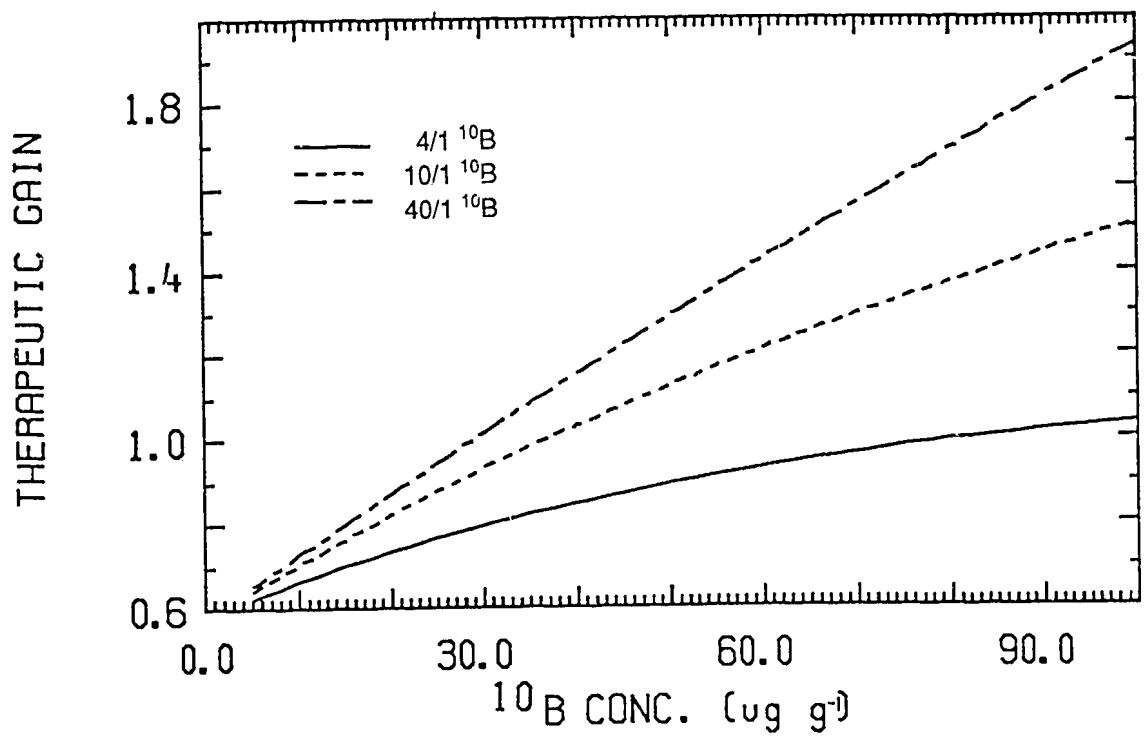

Figure 23 Therapeutic gain *v.* ^{10}B concentration for opposing neutron fields at 7.25 cm depth (12 cm AlF_3, 0.05 cm ^{6}LiF, 5 cm Pb)

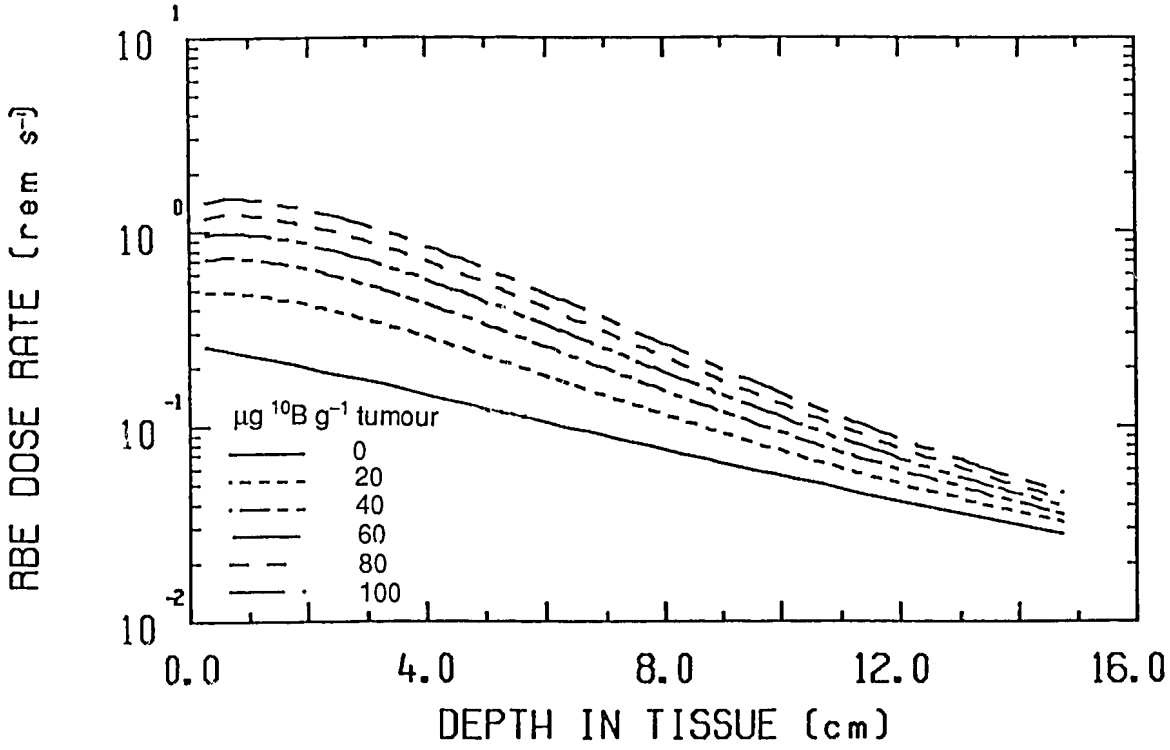

Figure 24 Tumour dose-depth curves for various ^{10}B loadings (^{10}B tumour/tissue ratio = 10.0)

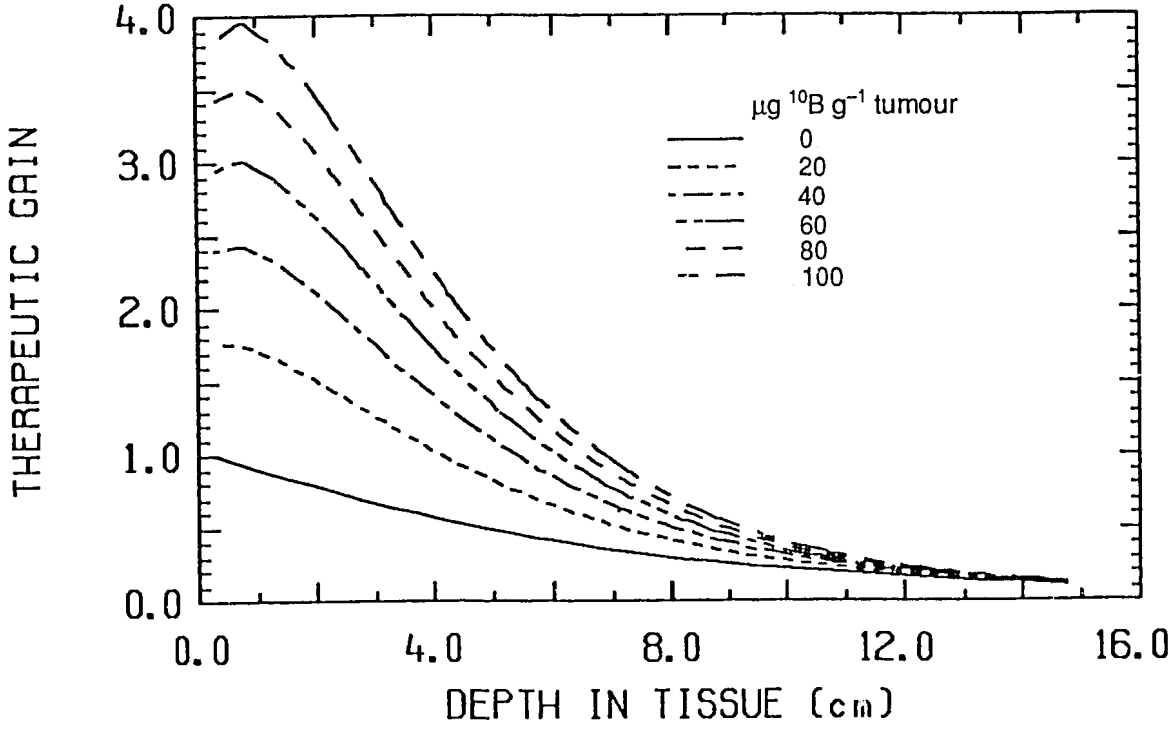

Figure 25 Therapeutic gain curves for various ^{10}B loadings (^{10}B tumour/tissue ratio = 10.0)

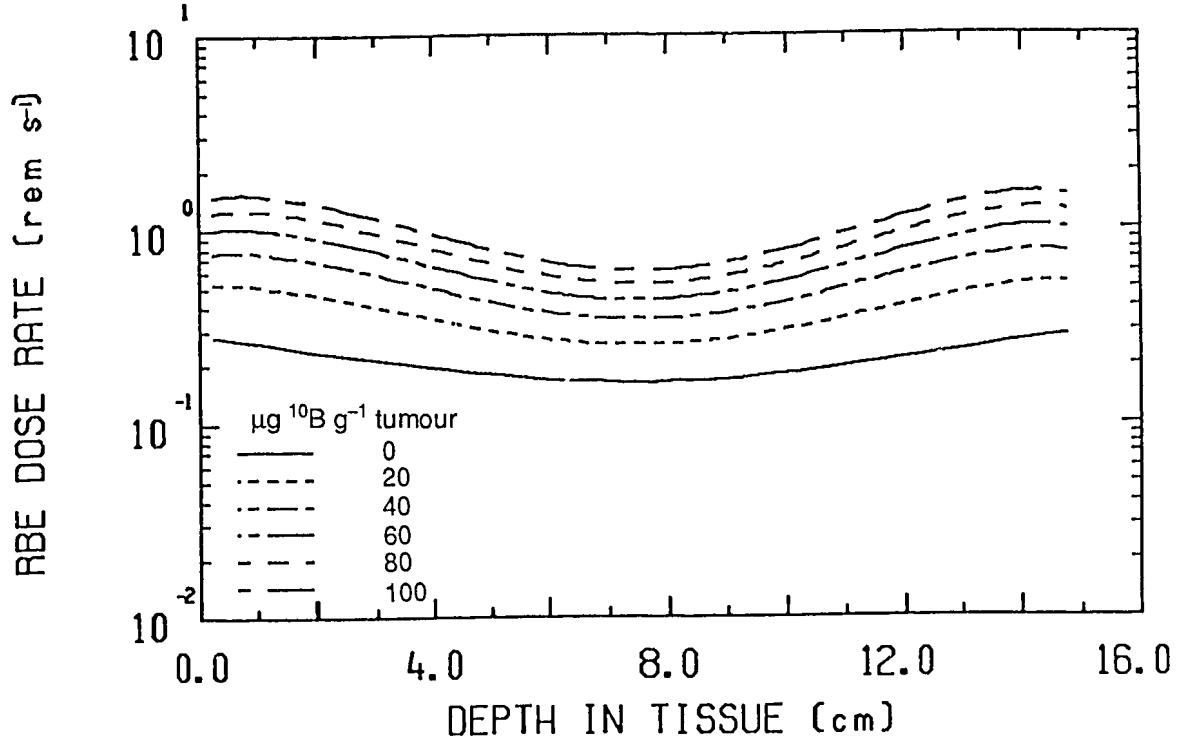

Figure 26 Tumour dose for opposing neutron fields (^{10}B tumour/tissue ratio = 10.0)

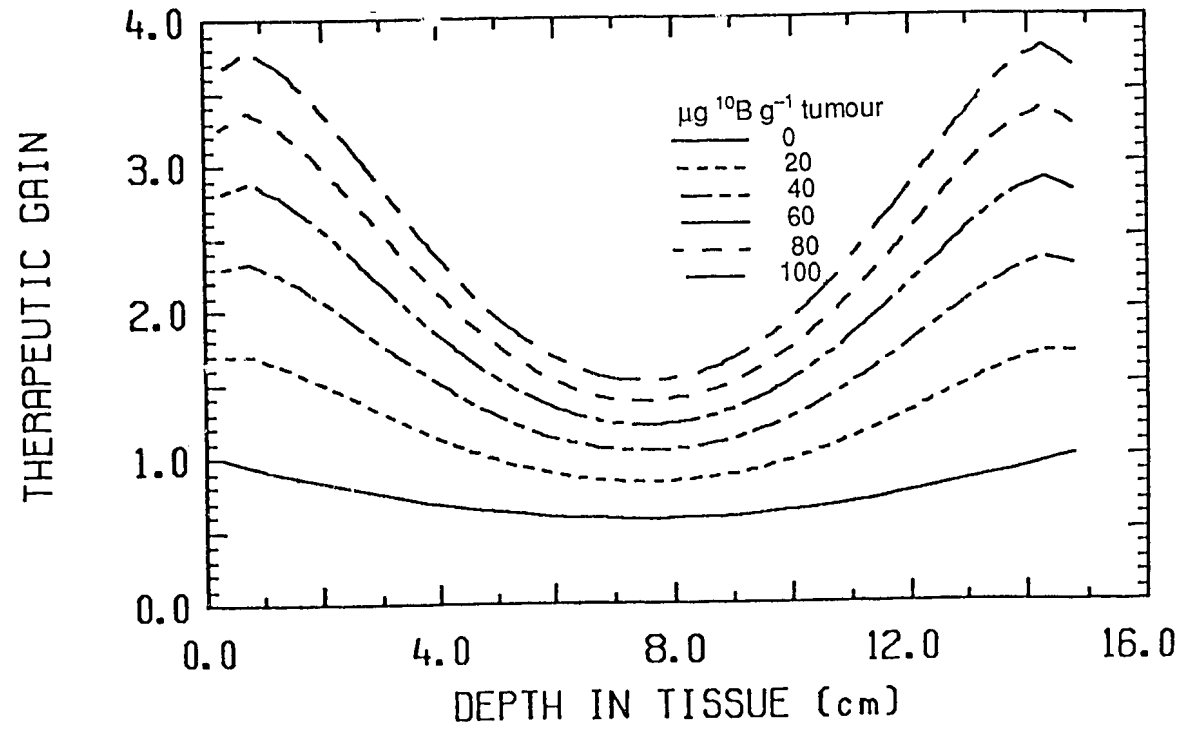

Figure 27 Therapeutic gain for opposing neutron fields (^{10}B tumour/tissue ratio = 10.0)